Ball Speed and Spin Estimation in Table Tennis using a Racket-mounted Inertial Sensor

Peter Blank, Benjamin H. Groh and Bjoern M. Eskofier
Digital Sports and Health Lab, Department of Computer Science,
Friedrich-Alexander University Erlangen-Nürnberg (FAU), Erlangen, Germany
Corresponding author: *peter.blank@fau.de*

ABSTRACT

In this paper, we present an approach for ball speed and spin estimation in table tennis based on a single racket-mounted inertial sensor. We conducted a research study comprising eight subjects performing different stroke types resulting in various ball speeds and spins. All ball-racket impacts were recorded with a high-speed camera for further evaluation. Firstly, several assumptions and simplifications of the unknown initial ball properties and the movements of player and racket had to be made. Secondly, the racket blade velocity right after impact was calculated. This was combined with a rebound model between the ball and the rubber to predict the speed and spin of the ball. Overall, the ball speed of strokes with forward spin could be estimated with an accuracy of $79.4\ \%$ and for strokes with backward spin with an accuracy of $87.4\ \%$. The spin was estimated with an accuracy of $73.5\ \%$ and $75.0\ \%$, respectively. To our knowledge, this contribution is the first attempt to estimate characteristics of rebounded balls with a single racket-mounted inertial sensor considering unknown initial conditions and constraints.

Author Keywords

inertial sensors; ball speed and spin estimation; movement analysis; table tennis

ACM Classification Keywords

I.5.4 Pattern Recognition: Applications: Signal processing

INTRODUCTION

Wearable sensors and devices are already successfully used in health, fitness and sports applications [14]. They opened new possibilities in data analysis techniques, since they can unobtrusively be integrated into any body-worn accessories like clothes, shoes, wristbands, smartphones, smartwatches or almost any sports equipment. For applications in sports science context, Wearables mostly consist of inertial measurement units (IMUs) based on accelerometers and gyroscopes. Therefore, Wearables represent an important data source for todays motion and movement analysis [14]. However, Wearables are not restricted to support professional athletes. They can also be used in amateur sports and educational applications, as well as for statistical surveys, entertainment and promotion purposes [1]. An additional advantage is that sensor-based analysis techniques can provide an objective view on different kinds of sports, for which it is often difficult to evaluate performance or technical correctness. This applies in particular, if additional sports equipment has to be used or motions are complex and dynamic, for example in running, athletics, football, basketball, badminton and (table) tennis.

Here, we focus on the application in table tennis. With many possible variations of strokes resulting in different ball speeds and spins, table tennis is a complex and challenging sport, making it an interesting and promising candidate for further investigation. Therefore, some research has already been done in this field using inertial or embedded sensors. In a previuos work [3] of our group it was shown, how stroke types could be detected and classified with a racket-mounted inertial sensor using machine learning algorithms. Different classifiers were evaluated concerning accuracy and complexity. Quantitative stroke analysis was done using a 3-dimensional accelerometer attached with a wristband in [12]. Stroke types from professional and amateur players were compared to prove their skill levels. An IMU sensor integrated into a table tennis racket was used in [5] to measure acceleration and angular velocity signals for visual and quantitative stroke analysis. In [4], the ball impact position on a table tennis racket was estimated using a model based time-difference-of-arrival distribution. Piezo-electric sensors were placed around the racket blade to capture impact vibrations.

So far, all approaches neither addressed ball speed nor spin estimation. In [10], a cricket ball was instrumented with a 3D gyroscope to determine its spin rate. Data was stored on an integrated memory and later processed for characterization of bowling deliveries. However, it is not possible to instrument a table tennis ball due to its very low weight. This is the reason for only vision based approaches of ball speed and spin measurements. In [11], the 3D spin rate of a table tennis ball was tracked using a 2D camera and a special quaternion motion filter. Another approach was made in [21]. The printed natural brand of a table tennis ball was tracked using a set of three cameras at different spots. Another approach was made by [19]. The ball spin was estimated while a 3D sphere model was registered to the table tennis surface.

In contrast to the mentioned video-based systems, our purpose was to develop a ball speed and spin estimation system based on only one single inertial sensor mounted at the table tennis racket. With this restriction, we had to make several

ISWC '17, September 11–15, 2017, Maui, HI, USA

ACM 978-1-4503-5188-1/17/09...$15.00
https://doi.org/10.1145/3123021.3123040

assumptions and simplifications for the initial unknown ball motion and the racket movement. Kinematic data based on acceleration and angular velocity was collected to estimate the rebounded ball speed and to predict the spin after impact.

METHODS

Video Data Labeling

As reference for evaluation of the speed and spin prediction, a suitable method for detecting ball properties from video frames during impact scenes had to be found. Due to high ball speeds of up to 30 $\frac{m}{s}$ and ball rotations of up to 800 $\frac{rad}{s}$ [13], cameras with high frame rates ($> 500\ Hz$) were necessary. This normally comes along with low resolutions and limited fields of view, which can lead to complex analyses. However, in this contribution we used an approach based on [20]. We modified and extended their algorithms. The ball speed v_b was determined by the pixel displacement of the ball center vectors $\vec{p}_A$ and $\vec{p}_B$ during two consecutive frames A and B. This was averaged over $N = 10$ frames, since the ball speed v_b was assumed to remain constant during this period. The pixel width in each frame $p_{w,i}$ (1) was calculated by $M = 4$ averaged envelopes (see Figure 1B) around the ball area A_b.

$$p_{w,i} = \frac{1}{M} \sum_{j=1}^{M} \sqrt{\frac{\pi}{A_{b,i,j}}} \tag{1}$$

With the known ball radius $r_b = 0.02\ m$ and the time difference $dt = 0.001\ s$ between two frames, the resulting ball speed v_b (2) could be written as follows.

$$v_b = \frac{r_b}{N \cdot dt} \sum_{i=1}^{N} \|\vec{p}_{B,i} - \vec{p}_{A,i}\| \cdot p_{w,i} \tag{2}$$

The ball spin was computed by the difference of consecutive feature point displacement vectors $\vec{x} = \vec{x}_B - \vec{x}_A$ and ball center translation vectors $\vec{p} = \vec{p}_B - \vec{p}_A$ during two video frames. Feature points could be any prominent point on the ball surface, which were trackable during all N frames (see Figure 1B). The distortion angle α_b (3) of the resulting vector between the coordinate axes represented the rotation angle.

$$\alpha_{b,i} = arccos\left(\frac{(\vec{x}_{A,i} - \vec{p}_{A,i}) \cdot (\vec{x}_{B,i} - \vec{p}_{B,i})}{\|\vec{x}_{A,i} - \vec{p}_{A,i}\| \cdot \|\vec{x}_{B,i} - \vec{p}_{B,i})\|}\right) \tag{3}$$

The final ball rotation ω_b was given by equation (4) with respect to the generated spin direction.

$$\omega_b = \frac{1}{N \cdot dt} \sum_{i=1}^{N} \frac{sgn[(\vec{x}_i - \vec{p}_i) \times (\vec{x}_{A,i} - \vec{p}_{A,i})]}{\alpha_{b,i}^{-1}} \tag{4}$$

Since we used a different high-speed camera and other ball features as in [20], we evaluated our method based on a pendulum approach, which can be seen in Figure 1A. A DC gear motor from *Maxon Motor* with a motor constant $D = 35.5\ \frac{turns}{Vs}$ and a gear ratio $G = 4.4$ was connected at the pendulum rod ($l = 0.45\ m$). The table tennis ball was precisley fixed at the motor axis to generate an accurate rotation speed ω_P (5) by the change of the motor voltage U.

$$\omega_P = 2 \cdot \pi \cdot \frac{D}{60} \cdot \frac{1}{G} \cdot U \tag{5}$$

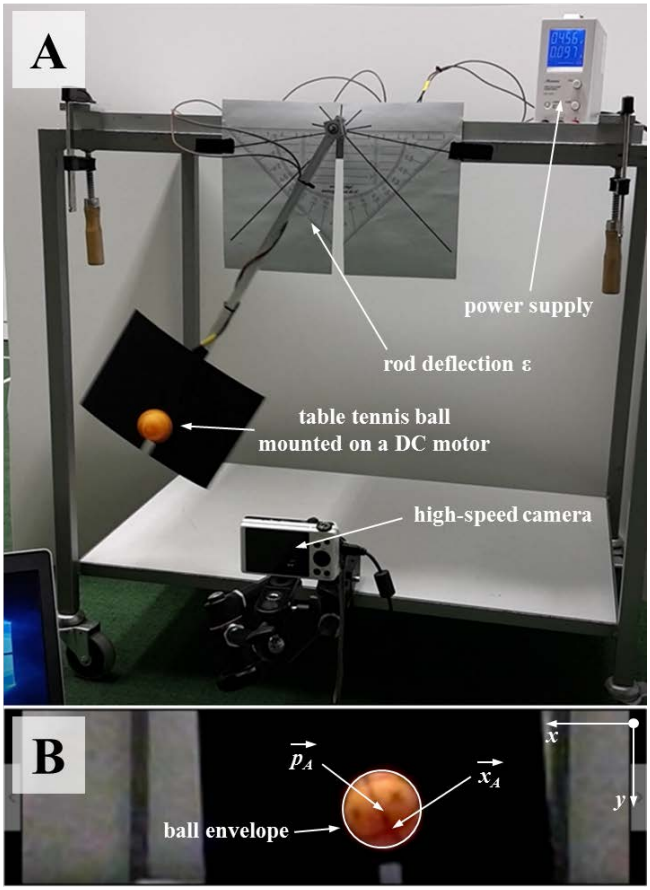

Figure 1. Upper figure (A): experimental pendulum approach for video labeling evaluation. The high speed camera was mounted in front of the pendulum's turning point, whereas the rod deflection determination is fixed at the rotation axis. The DC motor was connected to a power supply for precise voltage adjustment. Lower figure (B): typical high speed video frame, with a resolution of 224 x 64 pixels (see section *Study Design*). The surface of the table tennis ball is marked with different cross and line features. The ball center vector $\vec{p}_A$ is the center of the mapped ball envelope (white circle). The feature vector $\vec{x}_A$ can be any prominent trackable feature point (here: intersection between two prominent lines). All envelopes and feature points were labeled manually by a single expert to maintain a uniform data analysis.

The linear speed v_P of the ball was generated by a specific rod deflection angle ϵ. With the total mass $m = 0.614\ kg$ of the pendulum, the total inertia moment $J = 50.988 \cdot 10^{-3}\ kgm^2$ (sum of all single inertia moments) and the gravitational acceleration $g = 9.80665 \frac{m}{s^2}$, the pendulum speed at the turning point could be calculated with equation (6).

$$v_P = \sqrt{\frac{2 \cdot l^2 \cdot m \cdot g \cdot [l - cos(\epsilon) \cdot l]}{l^2 \cdot m + J}} \tag{6}$$

For a meaningful evaluation, we applied different linear speeds combined with different ball rotations. With the pendulum as reference, the proposed video labeling method achieved overall relative errors for the ball speed $f = -2.3\ \%$ and for the ball spin $f = -8.5\ \%$. The underestimated results could be interpreted as neglected friction or inadequate modeling of the inertia moment J. Furthermore, high pixel widths p_w due to the low camera resolution (section *Study Design*)

could contribute to these inaccuracies. However, the results were in the range of the original method [20] and even in the range of the other mentioned video-based approaches in [19] and [21]. This confirmed that our video labeling approach was suitable for ball speed and spin estimation.

Data Acquisition

Sensor Hardware

For the data collection, we used the IMU of the *miPod* sensor platform [2]. This measurement platform includes a triaxial acceleration sensor and a triaxial gyroscope resulting in a six-dimensional data set for each movement of player and racket. The accelerometer range and the gyroscope rate were set to $\pm$ 16 g and $\pm$ 2000 $\frac{deg}{s}$, respectively. Both sensors were sampled with 1000 Hz and a resolution of 16 $bits$ to capture all components of the expected highly dynamic motions. Every data acquisition contained a specified calibration routine similar to [9]. Accelerometers and gyroscopes were calibrated using six perpendicular static positions and three rotations about each sensor axis X, Y and Z. All obtained data (motion and calibration data) were stored during the data collection process on the internal flash memory and processed afterwards. Only one single IMU was placed into a milled cavity of the racket handle. Figure 2 exemplarily shows the sensor position and the corresponding axes. To avoid misalignments, the milled cavity has a slightly smaller negative contour of the sensor's outer dimensions for a tight fit. The prototype racket consists of a *XIOM Classic Allround S* blade and two *JOOLA energy X-tra 2.0 mm* rubbers.

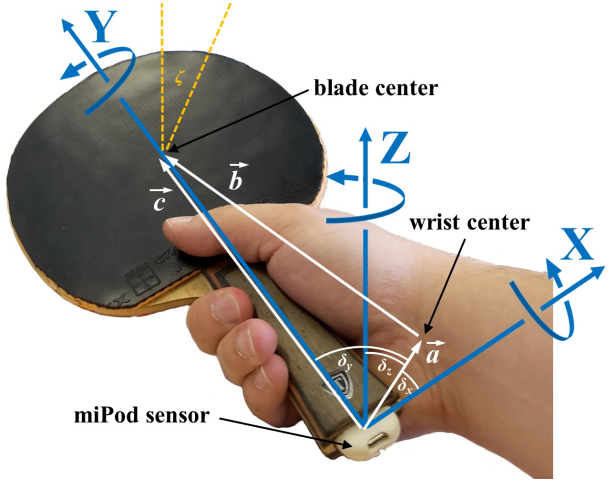

Figure 2. Example racket showing the sensor placement. The miPod sensor was mounted inside a milled cavity of the racket handle. The coordinate system (blue) is aligned to the main axes of the racket: X-axis and Y-axis span the main movement plain of most table tennis strokes (here: forehand drives, topspins and pushes). Main changes in spin become distinct in the rotation direction of the Z-axis. The impact force of the ball mainly affects also the signals in the Z-axis. Furthermore, the wrist rotation center is defined by $\vec{a}$ and the corresponding angles δ_x, δ_y and δ_z. The impact position is assumed to be the blade center $\vec{c}$. Moreover, the incident impact angle ζ is defined as the angle between the initial ball direction and the Z-axis (referring section *Ball and Racket Motion Assumption* and *Racket Speed Calculation*).

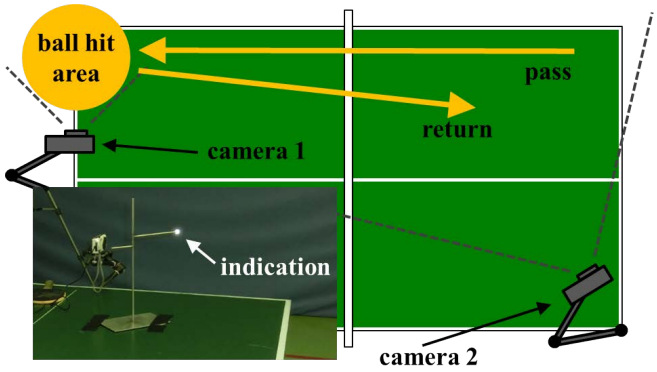

Figure 3. Schematic representation of the data collection exercises: there was a parallel pass from the upper right corner of the table to the ball hit area. Every player performed strokes with backward spin (pushes) and forward spin (drives and topspins) and returned the ball into the upper right quadrant of the table. Camera 1 provided visual data for labeling ball speed and ball spin, while camera 2 monitored the overall scene and the ball return positions. To provide visual support for the players during the exercises, a marker was mounted above the table to indicate the outer border of the ball hit area above the table surface.

Study Design

A research study was conducted to collect racket movement data of different stroke types from eight players. All subjects were male within an age range of 13 and 50 years. One subject was left-handed, whereas seven subjects were right-handed. All players used the same shakehand grip. The participants were members of the German national table tennis association. They were split into four higher and four lower level players, according to their current ranking coefficient [8]. We intentionally asked subjects with different playing abilities to receive a high variability in racket motions and therefore in different resulting ball speeds and spins.

A schematic of the data collection exercises can be seen in Figure 3. Firstly, the subjects had to perform forehand pushes with backward spin (P) from a parallel passed ball with a low backward spin inside a narrow hit area at the left upper corner of the table tennis table. The ball had to be returned into the right upper quadrant of the table. As a result, we assumed that the direction of the generated ball speed is parallel towards the image plane of camera 1. Additionally, we assumed that by far the largest part of the generated spin is perpendicular to the flight direction of the ball and therefore also perpendicular to the image plane of camera 1. Secondly, the players performed strokes with forward spin as forehand drives (D) or forehand topspins (T) from a passed ball with a low forward spin in the same manner. The video reference for ball speed and spin was provided by camera 1, a CASIO® Exilim HS-ZR300 high speed camera with a frame rate of 1000 Hz and a resolution of 224 x 64 pixels. Since the resolution was relatively low, the camera position and ball hit area were close to each other. The second camera (camera 2), a CASIO® Exilim HS-ZR200 with 120 Hz and a resolution of 640 x 480 pixels provided a scene overview and finally the verification of the ball return positions. All balls had special trackable features and patterns on their surface.

Ball and Racket Motion Assumptions

Because of the restricted access to comprehensive motion definition using only one single racket-mounted sensor, several assumptions had to be made, which affected the final ball speed and spin estimation. First of all, it was not intended to use knowledge about the ball speed $\vec{v}_{b,1}$ and spin $\vec{\omega}_{b,1}$ before impact. According to existing rebound models between balls and rubbers [15] or tables [7] on which we built on, these parameters are yet necessary. Therefore we assumed with (A1), that the incoming ball speed $\vec{v}_{b,1}$ is the corresponding racket speed $\vec{v}_R$ in contrary direction added with a mean velocity $\vec{\bar{v}}_\mu$ of all equal stroke types depending on each player. The initial ball spin $\vec{\omega}_1$ is stated as the parallel rotation $\vec{\omega}_R$.

(A1) $\vec{v}_{b,1} = -\big(\vec{v}_R + \vec{\bar{v}}_\mu\big), \quad \vec{\omega}_{b,1} = \big(\vec{\omega}_R\big)$

Since it is not possible to generate ball rotations in the orthogonal blade direction, the Z-component of $\vec{\omega}_R$ is set to $\omega_{R(z)} = 0$. Another unknown parameter is the incident impact angle ζ (see Figure 2), because it influences the addition of $\vec{\bar{v}_\mu}$. Based on video analysis, ζ was set to $45°$ for topspins and drives and $30°$ for backspin strokes of all players (A2).

(A2) $\zeta_{T,D} = 45°, \quad \zeta_P = 30°$

With (A3) we assumed further, that the ball impact position on the racket $\vec{c}$ is centered on the forehand side of the blade surface (also shown in Figure 2). With the dimensions of the blade, the ball impact coordinate is given as follows.

(A3) $\vec{c} = [0 \;\; 0.19 \;\; 0.007]^T \; [m]$

Since we are not able to describe the whole complex motion of a table tennis stroke using one single racket-mounted sensor, we strongly simplified the general differential equations in such a way (A4), that $\vec{v}_R$ consists of a linear and a rotational component. These parts can then be calculated by integration of the gravity compensated acceleration $\vec{\tilde{a}}(t)$ and the derivative of the angular velocity $\vec{\omega}(t)$, transformed by a wrist rotation matrix $\mathcal{W}$. Furthermore, we assumed that wrist rotations were the most prominent rotational parts and that other movements like arm or body rotations only had less influence on the final speed estimation.

(A4) $\vec{v_R} = \int \vec{\tilde{a}}(t) \cdot dt + \frac{d}{dt}\big(\mathcal{W} \cdot \vec{\omega}(t)\big)$

Finally, we determined a starting point x_m with minimal motion, which indicates the turning point of the performed stroke countermovement. At x_m we assumed (A5), that the overall acceleration $\vec{a}_i$ is equal to the gravitational acceleration g and that there is no further racket motion $\vec{v}_R$.

(A5) $\|\vec{a}(x_m)\| = g, \quad \vec{v}_R(x_m) = \vec{0}$

Moreover, we investigated other indicators for x_m, like global minima in the overall racket speed per data window before an impact or zero-crossings in the rotation axis orthogonal to the racket blade (X-axis). However, these showed worse results and were not considered further.

In summary, we specified these assumption to be independent from any subject physiology and any skill level, since all parameters locating the wrist center (see Figure 2) were averaged and speed and spin generation are exclusively determined by physical movement and rubber properties.

Racket Speed Calculation

The racket motion calculation is based on the 6-dimensional data of the accelerometer $\vec{a}$ and the gyroscope $\vec{\omega}$. With respect to the ball-racket impacts x_{ip} of each stroke and subject, the time-series data was split into windows $[x_{ip} - 1.2\ s,\ x_{ip} + 0.3\ s]$. The data window was intentionally moved more to the past, because prior countermovements contain the most important information about the type and the properties of a stroke [18]. x_m and x_{ip} were calculated using the root signal energy $E(i)$ (7) from the accelerometer X-axis $a_x(i)$, Y-axis $a_y(i)$ and Z-axis $a_z(i)$, where L is the window length and i the sample value.

$$E(i) = \sqrt{a_x(i)^2 + a_y(i)^2 + a_z(i)^2} \qquad 0 \leq i < L \tag{7}$$

Next, x_m is found by minimizing the difference between $E(i)$ and the gravitational acceleration $g = 9.80665 \frac{m}{s^2}$ (8).

$$x_m = argmin\big[E(i) - g\big] \tag{8}$$

Then, the exact impact position x_{ip} was calculated using a robust event and peak detection algorithm similar to [17]. Post-processing steps retained only the one peak, which had the highest energy $E(i)$. This indicated the most likely impact point x_{ip} (9). x_m and x_{ip} can be seen in Figure 4.

$$x_{ip} = argmax\big[E(i)\big] \tag{9}$$

In the next step, the linear velocity component $\vec{v}_{lR}(i)$ of the racket speed $\vec{v}_R(i)$ was calculated by integration of the acceleration from x_m to x_{ip}. However, the gravitational component of the measured acceleration had to be eliminated beforehand. First, a low-pass Butterworth filter with an order of $n = 1$ was used to suppress high frequency motion artifacts. According to [18], a cut-off frequency of $f_c = 25\ Hz$ was chosen. The filter was applied in a forward-backward manner to avoid any filter delay. Considering assumption (A5), the initial gravity vector $\vec{g}_m$ was equal to the acceleration vector $\vec{a}_m$ at point x_m. While integrating the angular velocity $\vec{\omega}(i)$, it was possible to estimate the relative angles $\vec{\phi}(i) = [\Delta\alpha(i)\ \Delta\beta(i)\ \Delta\gamma(i)]^T$ (10) of the racket during its motion per time interval $dt = 0.001\ s$.

$$\vec{\phi}(i) = \vec{\omega}(i) \cdot dt \qquad x_m \leq i < x_{ip} \tag{10}$$

According to the relative angles, the gravity vector $\vec{g}(i)$ could be sample-wise rotated by standard rotational matrices $\mathcal{R}_{\Delta\alpha}(i)$ for the X-axis, $\mathcal{R}_{\Delta\beta}(i)$ for Y-axis and $\mathcal{R}_{\Delta\delta}(i)$ for the Z-axis and finally be subtracted from the acceleration vector $\vec{a}(i)$ to get the gravity compensated acceleration $\vec{\tilde{a}}(i)$ (11).

$$\vec{\tilde{a}}(i) = \vec{a}(i) - \mathcal{R}_{\Delta\gamma}(i) \cdot \big[\mathcal{R}_{\Delta\beta}(i) \cdot \big[\mathcal{R}_{\Delta\alpha}(i) \cdot \vec{g}(i)\big]\big] \qquad x_m \leq i < x_{ip} \tag{11}$$

Finally with assumption (A5), the compensated acceleration $\vec{\tilde{a}}(i)$ (12) was integrated from x_m to x_{ip} starting with

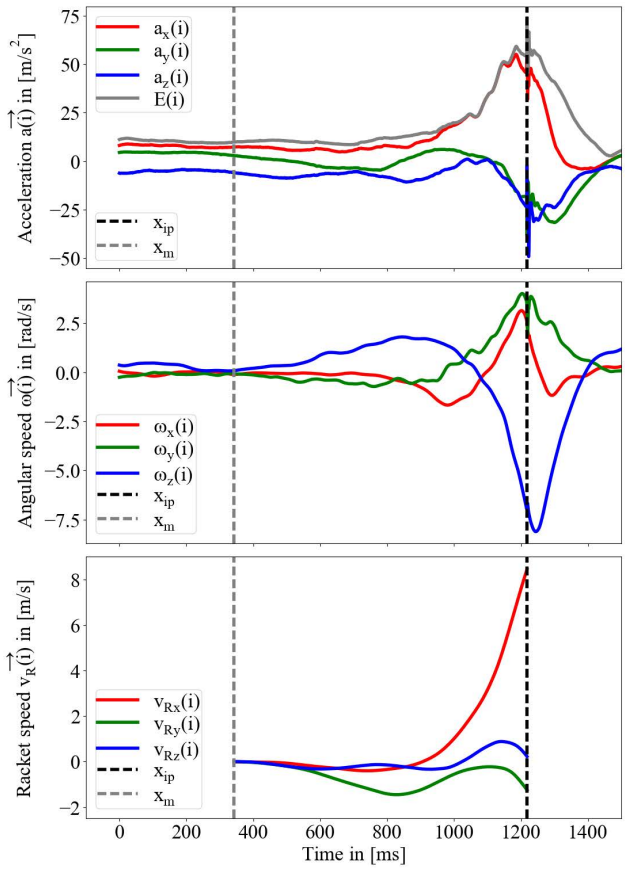

Figure 4. The two upper figures show the raw acceleration $\vec{a}(i)$ and the angular speed $\vec{\omega}(i)$ of an example topspin and drive stroke in $[\frac{m}{s^2}]$ and $[\frac{rad}{s}]$, respectively. Additionally, the root signal energy $E(i)$ is shown in gray. x_m (motionless point) and x_{ip} (impact) are marked as dotted gray and black lines. It can be seen, that x_m is located were $E(i)$ is closest to the gravitational acceleration g before impact x_{ip}, which should indicate almost no motion. This is also confirmed by nearly zero angular speed at x_m. The lower figure indicates the racket speed $\vec{v}_R(i)$ in $[\frac{m}{s}]$. It is the sum of linear speed $\vec{v}_{lR}(i)$ and transformed rotational speed $\vec{v}_{rR}(i)$. All data is split into X-axis (red), Y-axis (green) and Z-axis (blue).

$\vec{v}_{lR}(0) = \vec{0}$ to obtain the absolute linear speed $\vec{v}_{lR}(i)$.

$$\vec{v}_{lR}(i) = \vec{v}_{lR}(0) + \int_{x_m}^{x_{ip}} \vec{a}(i) \cdot dt \qquad x_m \leq i < x_{ip} \tag{12}$$

According to (A4), the rotational component $\vec{v}_{rR}(i)$ (13) of the racket speed $\vec{v}_R(i)$ is mainly based on the rotation of the wrist. Therefore, the tangential velocities of all frame axes were transformed considering the principle of lever to the blade center $\vec{c}$ using the transformation matrix $\mathcal{W}$ (14). The wrist position was determined using the enclosed angles $\vec{\delta} = [\delta_x\ \delta_y\ \delta_z]^T$ from the racket coordinate origin to the associated axes and the distances $\vec{a} = [a_x\ a_y\ a_z]^T$, respectively in the XY-plane, the YZ-plane and the XZ-plane (see Figure 2).

$$\vec{v}_{rR}(i) = \mathcal{W} \cdot \vec{\omega}(i) \qquad x_m \leq i < x_{ip} \tag{13}$$

$$\mathcal{W} = \begin{bmatrix} 0 & a_z\ cos(b_z) & a_x\ cos(b_x) \\ a_y\ sin(b_y) & 0 & a_x\ sin(b_x) \\ -a_y\ cos(b_y) & a_z\ sin(b_z) & 0 \end{bmatrix}$$
$$b_j = \frac{a_j \cdot arcsin(\frac{\pi}{2} - \delta_j)}{\sqrt{c_j^2 + a_j^2 - 2 \cdot c_j \cdot a_j \cdot cos(\frac{\pi}{2} - \delta_j)}} \qquad j \in \{x, y, z\} \tag{14}$$

Due to a different body physiology of all subjects, the parameters $\vec{a}$ and $\vec{\delta}$ were measured individually for every subject and finally averaged. Conclusively, the racket speed $\vec{v}_R$ shortly after impact x_{ip} is given as the sum of the linear speed $\vec{v}_{lR}(i)$ and the transformed rotational speed $\vec{v}_{rR}(i)$ (15). It is illustrated in Figure 4 for a topspin and drive stroke. Additionally, the racket rotation is given as the angular velocity $\vec{\omega}_R$ at time x_{ip} (16).

$$\vec{v}_R = \left(\vec{v}_{lR}(i) + \vec{v}_{rR}(i)\right)\big|_{i\,=\,x_{ip}} \tag{15}$$

$$\vec{\omega}_R = \vec{\omega}(i)|_{i\,=\,x_{ip}} \tag{16}$$

Rebound Model

Our approach is based on the rebound models in [15] and [16]. Ball speed and spin estimation after impact depends not only on the initial ball speed and spin, but also on special characteristics of the used rubber. One parameter is the restitution coefficient e_R (17) between ball and racket. It is defined as the energy loss during the elastic ball impact and can be calculated by measuring the height before impact h_1 and the height after impact h_2 during a free fall [6].

$$e_R = \sqrt{\frac{h_2}{h_1}} \tag{17}$$

Here, we averaged ten trials for the used racket and rubber combination. Another parameter is the friction cofficient μ_R (18). It was calculated as the quotient of force meter measures F_R and the normal force of a known test mass F_N fixed on a table tennis ball during the sliding over the rubber surface.

$$\mu_R = \frac{F_R}{F_N} \tag{18}$$

$$1 - \frac{5}{2} \cdot \mu_R \cdot (1 + e_R) \cdot \frac{|v_{b,1(z)}|}{\|\vec{v}_{b,1(xy)}\|} > 0 \tag{19}$$

If equation (19) is fulfilled, the table tennis ball is sliding over the rubber surface during an impact. Since the friction coefficient is always high enough, the ball will usually roll during the impact. Therefore, the sliding case was not considered further. As mentioned in [15], the actual impact is modeled as a virtual spring-absorber system, which saves and releases energy during the impact process. This was modeled by the parameter k_p (20). Since the impact duration t_{ip}, the total displaced mass m_r and the spring constant k_r were hard to obtain, k_p was modeled with a fifth degree polynomial for topspins and drives and with a third degree polynomial for pushes.

$$k_p = \frac{t_{ip}}{2} \cdot \sqrt{m_r \cdot k_r} \tag{20}$$

We used two separate functions because we expected differences in the impact duration and rubber deformation behaviour within different stroke types. The resulting parameters $k_{p(T,D)}$ and $k_{p(P)}$ were found using a least squares minimization method equally for all players. With the known ball mass $m_b = 0.0027\ kg$ and the known ball radius $r_b = 0.02\ m$, ball speed $\vec{v}_{b,2}$ and spin $\vec{\omega}_{b,2}$ after impact could be finally calculated.

$$\vec{v}_{b,2} = \mathcal{A} \cdot \vec{v}_{b,1} + \mathcal{B} \cdot \vec{\omega}_{b,1} \tag{21}$$

$$\vec{\omega}_{b,2} = \mathcal{C} \cdot \vec{v}_{b,1} + \mathcal{D} \cdot \vec{\omega}_{b,1} \tag{22}$$

$$\mathcal{A} = \begin{bmatrix} 1-k_{pv} & 0 & 0 \\ 0 & 1-k_{pv} & 0 \\ 0 & 0 & -e_R \end{bmatrix}, \mathcal{B} = k_{pv} \cdot \begin{bmatrix} 0 & r_b & 0 \\ -r_b & 0 & 0 \\ 0 & 0 & 0 \end{bmatrix}$$

$$\mathcal{C} = k_{p\omega} \cdot \begin{bmatrix} 0 & -\frac{1}{r_b} & 0 \\ \frac{1}{r_b} & 0 & 0 \\ 0 & 0 & 0 \end{bmatrix}, \mathcal{D} = \begin{bmatrix} 1-k_{p\omega} & 0 & 0 \\ 0 & 1-k_{p\omega} & 0 \\ 0 & 0 & 1 \end{bmatrix}$$

$$k_{pv} = \frac{k_p}{m_b}, \quad k_{p\omega} = \frac{3 \cdot k_p}{2 \cdot m_b}$$

Evaluation

With equations (21) and (22) and assumptions (A1) to (A5) it was possible to estimate the resulting ball speed $v_{\vec{b},2}$ and spin $\omega_{\vec{b},2}$. With respect to the study design and the camera orientation (ball speed parallel towards the image plane), the labeled ball speed v_b was approximately the estimated ball speed in the XZ-plane of the racket frame.

$$v_b \approx v_{b,2(xz)} = \sqrt{v_{b,2(x)}^2 + v_{b,2(z)}^2} \tag{23}$$

Similarly, the labeled ball spin ω_b is approximately the estimated ball spin of the Y-axis alongside the racket handle (rotation orthogonal to the image plane).

$$\omega_b \approx \omega_{b,2(y)} \tag{24}$$

As evaluation measure, we used mean and standard deviation, overall accuracy and qualitative diagrams to compare labeled and estimated data. With the assumptions, $\vec{\delta}$ was defined as $[25\ 60\ -20]^T\ [^\circ]$ for the enclosed wrist angles, $\vec{a}$ was calculated as $[-0.055\ 0.035\ 0.045]^T\ [m]$ for the averaged wrist distances and $\vec{c}$ was determined as $[0\ 0.19\ 0.007]^T\ [m]$ for the blade center. The friction coefficient μ_R was calculated as 1.533, the restitution e_R as 0.746, the topspin and drive k-parameter $k_{p(T,D)}$ and the push stroke k-parameter $k_{p(P)}$ as $1.625 \cdot 10^{-3}\ kg$ and $1.76 \cdot 10^{-3}\ kg$, respectively.

RESULTS

In total, we collected ball speed and spin data from 109 valid impacts (entire impact scene visible in camera 1 and ball return position inside correct table quadrant). The results of the estimated ball speeds $v_{b,2(xz)}$ and spins $\omega_{b,2(y)}$ can be seen in Figure 5. Additionally, Figure 6 represent a graphical method to compare the estimated results with the labeled data. Table 1 show results individually for ball spin $v_{b,2(xz)}$ and ball speed $\omega_{b,2(y)}$.

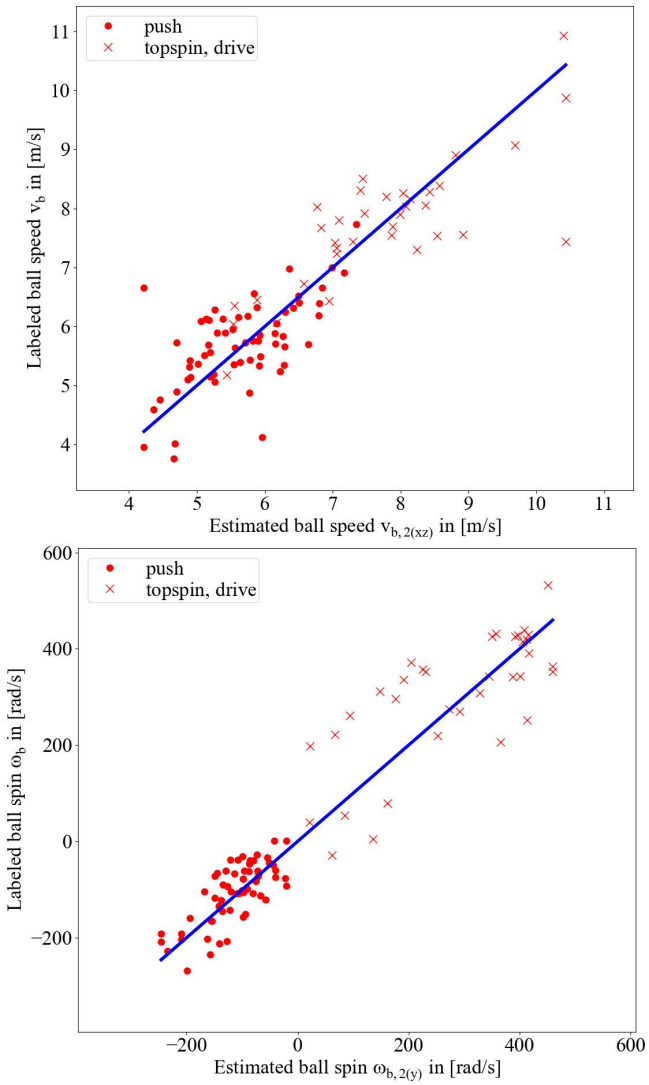

Figure 5. The estimated ball speed $v_{b,2(xz)}$ in $[\frac{m}{s}]$ (upper figure) and estimated ball spin $\omega_{b,2(y)}$ in $[\frac{rad}{s}]$ (lower figure) are plotted against the labeled ball speed v_b and labeled ball spin ω_b, respectively. Topspin and drive strokes are marked as red crosses, whereas pushes marked as red dots. The blue line would indicate an ideal estimation. Negative rotations indicate backward, positive values forward spin.

Stroke	$v_{b,2(xz)}\ [\frac{m}{s}]$	[%]	$\omega_{b,2(y)}\ [\frac{rad}{s}]$	[%]
T, D	-0.09 ± 0.59	79.4	-22.40 ± 95.78	73.5
P	-0.01 ± 0.57	87.4	-6.03 ± 41.99	75.0

Table 1. Results given for the ball speed $v_{b,2(xz)}$ in $[\frac{m}{s}]$ and for the ball spin $\omega_{b,2(y)}$ in $[\frac{rad}{s}]$ as well as for mean μ and for standard deviation σ, split into topspin (T), drive (D) and push (P) strokes. Moreover, the total accuracy is given in [%].

DISCUSSION

The results confirm, that it is possible to estimate the ball speed and spin with only one IMU mounted inside a table tennis racket. Despite all assumptions and simplifications, the ball speed of topspin and drive strokes could be estimated with an accuracy of 79.4 % (-0.09 ± 0.59 $\frac{m}{s}$) and for pushes

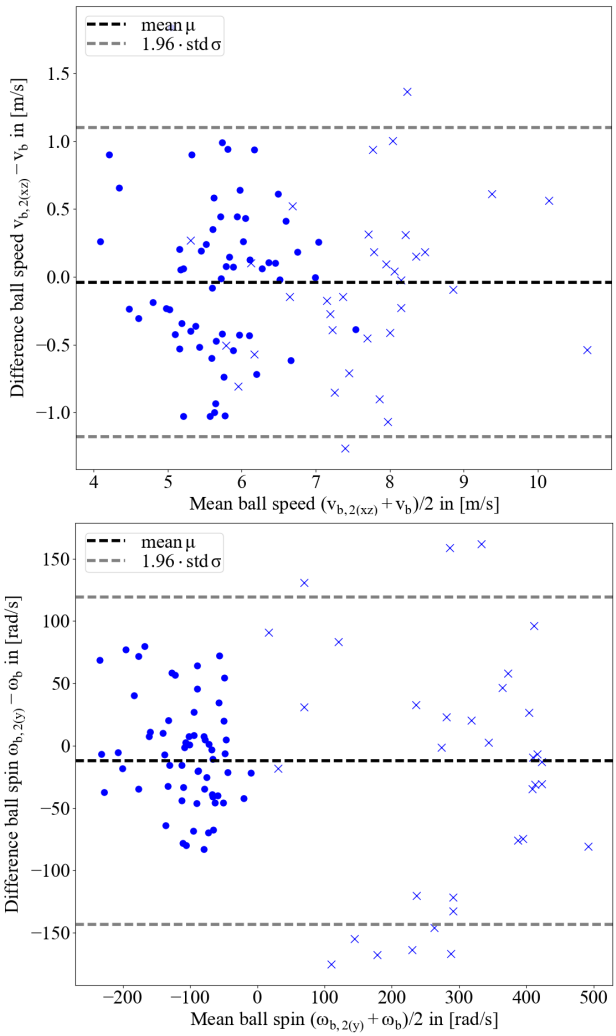

Figure 6. In the upper figure, the ball speed differences $v_{b,2(xz)} - v_b$ of estimated and labeled data are plotted against the mean $0.5 \cdot (v_{b,2(xz)} + v_b)$ of both values. In the lower figure, the ball spin differences $\omega_{b,2(xz)} - \omega_b$ of estimated and labeled data is plotted against the mean $0.5 \cdot (\omega_{b,2(xz)} + \omega_b)$ of both values. The mean μ of the differences is shown as dotted black line, whereas the 1.96-fold standard deviations σ are shown in dotted gray lines. Blue crosses are topspins or drives, blue dots represent push strokes.

of 87.4 % (-0.01 $\pm$ 0.57 $\frac{m}{s}$). The ball spin could be estimated with 73.5 % (-22.40 $\pm$ 95.78 $\frac{rad}{s}$) for topspins and drives and 75.0 % (-6.03 $\pm$ 41.99 $\frac{rad}{s}$) for pushes.

Other ball spin estimation approaches using video labeling like [11], [19] or [21] show an overall accuracy of 80 % to 95 %, depending on expenditure and complexity of the methods. On the one hand, this single sensor approach has slightly less accuracy regarding the spin estimation. On the other hand, the ball speed estimation shows slightly better results in comparison to existing methods like [15] or [16], which achieve an overall speed accuracy of 70 % to 85 %.

However, for all results the standard deviations are clearly higher than the mean values, which indicates a high error distribution. This is particularly the case for high ball rotations during topspins or drives (red crosses in Figure 5 and wide spread of blue crosses in Figure 6). This could be caused due to the mutual conversion of ball speed and spin during the impact. With (A1) we suggest an average value $\vec{v}_\mu$ for the unknown incoming ball speed depending on the stroke type, but in reality, this is only a rough estimation for some return cases and causes outliers in the speed distribution. For example, a topspin can be performed in flatter or steeper ways with more or less similar racket speed. Another example is, that a topspin can be performed as a return of a topspin itself (fast incoming ball speed) or of a push (low incoming ball speed). In addition, we considered only fixed incident impact angles ζ (A2). But ζ has influence on the component-wise addition of $\vec{v}_\mu$ with the racket speed $\vec{v}_R$. The consequence is, that both factors contribute to either a high error distribution or good value estimates and lead to underestimated ball speed and spin results over all strokes (see Table 1). In contrast, high speed values and low rotations were better predicted, since there was no large variety in motion based on the players ability. According to Figure 6, no bias drift, systematical or value-dependent errors between video-based and sensor-based estimation are visible. Nevertheless, the tendency (higher values as higher ones, lower values as lower ones) of ball speeds and spins was well estimated.

According to the video data, ball impact positions were spread over the whole racket blade, independent of any stroke type. However, we defined the impact position $\vec{c}$ as static (A3). Thus, the wrist transformation matrix $\mathcal{W}$ was imprecise and caused wrong calculations of angular velocity components. Modifying the racket and physiological wrist parameter $\vec{c}$, $\vec{\delta}$ and $\vec{a}$ gives an detailed insight into the influence to $\mathcal{W}$ and the final accuracy. A 10° deviation of $\vec{\delta}$ and 10 mm for $\vec{c}$ and $\vec{a}$ in the Z-axis causes less than 1 % error of the angular velocity component. However, deviations for $\vec{c}$ and $\vec{a}$ in the X- and Y-axis of 10 mm cause errors of 15 %, since X and Y define the impact position. In future, it could be better estimated with the ball impact localization approach in [4].

In our view, the primary sources of inaccuracies are the strongly simplified motion equations (A4) and the estimation of x_m as starting point for integration, resulting in only rough speed and spin estimations. Additionally, we assumed that there was no racket motion at x_m. But this did not include linear motion during the countermovements, which are not recognizable with the accelerometer or the gyroscope. For that, we needed a known resting point in the world frame, but only had inertial data in the local and moving racket frame. However, the intention of this approach is not to provide an exact description of racket movements resulting in accurate ball properties, but to proof that it is possible to apply different assumptions and simplifications for unknown occurrences to estimate the ball speed and spin shortly after impact.

SUMMARY AND OUTLOOK

In this contribution, we presented an approach for ball speed and spin estimation in table tennis using only one single inertial sensor mounted inside a table tennis racket. We conducted a research study with eight subjects performing differ-

ent stroke types (topspins, drives and pushes) resulting in various ball speeds and spins, including forward and backward spins. All impacts were recorded with a high-speed camera for evaluation. Using assumptions and simplifications of the initial ball motion and racket movement, we could estimate the ball speed and spin right after impact. The results showed, that the ball speed of strokes with forward spin were predicted with an accuracy of $79.4\,\%$ and for strokes with backward spin with an accuracy of $87.4\,\%$. The spin was estimated with an accuracy of $73.5\,\%$ and of $75.0\,\%$, respectively.

In the future, we will adapt the assumptions to better reflect the racket movement, starting from a well chosen resting point for the racket motions to initial unknown ball properties. We will also implement filter-based approaches to estimate the racket motion during the impact more precisely. Together with other sensor-based systems like stroke classification [3] or ball impact localization [4], it will finally be integrated into an instrumented racket. Practically, the system can be used by table tennis beginners and professionals during training sessions and matches to analyze techniques and tactics.

ACKNOWLEDGMENTS

We thank the table tennis club SpVgg Erlangen. This work was supported by the Bavarian Ministry for Economic Affairs, Infrastructure, Transport and Technology and the Embedded Systems Initiative (ESI). Bjoern M. Eskofier gratefully acknowledges the support of the German Research Foundation (DFG) within the framework of the Heisenberg professorship programme (grant number ES 434/8-1).

REFERENCES

1. Baca, A., and Kornfeind, P. Rapid feedback systems for elite sports training. *Pervasive Computing vol. 5*, no. 4 (2006), pp. 70–76.
2. Blank, P., Kugler, P., Schlarb, H., and Eskofier, B. M. A wearable sensor system for sports and fitness applications. In *Proc. of the Annual Congress of the European College of Sports Sciences* (2014), pp. 703.
3. Blank, P. and Hoßbach, J. and Schuldhaus, D. and Eskofier, B.M. Sensor-based stroke detection and stroke type classification in table tennis. In *Proc. of Int. Symp. on Wearable Computers* (2015), pp. 93–100.
4. Blank, P. and Kautz, T. and Eskofier, B.M. Ball impact localization on table tennis rackets using piezo-electric sensors. In *Proc. of Int. Symp. on Wearable Computers* (2016), pp. 72–79.
5. Boyer, E., Bevilacqua, F., Phal, F., and Hanneton, S. Low-cost motion sensing of table tennis players for real time feedback. *Int. J. of Table Tennis Sci. vol. 8* (2013).
6. Briggs, L. J. Methods for measuring the coefficient of restitution and the spin of a ball. *J. of Research of the National U.S. Bureau of Stds. vol. 34* (1945), pp. 1–21.
7. Chen, X., Tian, Y., Huang, Q., Zhang, W., and Yu, Z. Dynamic model based ball trajectory prediction for a robot ping-pong player. In *Proc. of the Int. Conf. on Robotics and Biomimetics* (2010), pp. 603–608.
8. Deutscher Tischtennis-Bund e.V. *Beschreibung der JOOLA-Rangliste*, 19 ed. Deutscher Tischtennis-Bund e.V., 2015.
9. Ferraris F. and Grimaldi U. and Parvis, M. Procedure for effortless infield calibration of three-axial rate gyro and accelerometers. *Sensors and Materials vol. 7*, no. 5 (1995), pp. 311–330.
10. Fuss, F. K. and Smith, R. M and Subic, S. Determination of spin rate and axes with an instrumented cricket ball. In *Proc. of Int. Conf. on Eng. of Sports*, pp. 128–133.
11. Glover, J. and Kaelbling, L. P. Tracking the spin on a ping pong ball with the quaternion bingham filter. In *Proc. of Int. Conf. on Robotics and Automation*, pp. 4133–4140.
12. Guo, Y.-W., Liu, G.-Z., Huang, B.-Y., Zhao, G.-R., Mei, Z.-Y., and Wang, L. A pilot study on quantitative analysis for table tennis block using a 3d accelerometer. In *Proc. of the Int. Conf. on Information Technology and Applications in Biomedicine* (2010), pp. 1–4.
13. McAfee, R. *Table Tennis, Steps to Success*. Human Kinetics, Inc., 2009.
14. McCann, J., and Bryson, D. *Smart Clothes and Wearable Technology*. Elsevier, 2009.
15. Nakashima, A., Kobayashi, Y., Ogawa, Y., and Hayakawa, Y. Modeling of rebound phenomenon between ball and racket rubber with spinning effect. In *Proc. of the ICCAS-SICE Int. Joint Conference* (2009), pp. 2295–2300.
16. Nakashima, A., Ogawa, Y., Kobayashi, Y., and Hayakawa, Y. Modeling of rebound phenomenon of a rigid ball with friction and elastic effects. In *Proc. of the American Control Conf.* (2010), pp. 1410–1415.
17. Palshikar, G. Simple algorithms for peak detection in time-series. In *In Proc. of the Int. Conf. of Adv. Data Analysis, Business Analytics and Intelligence* (2009).
18. Rodrigues, S. T., Vickers, J. N., and Williams, A. M. Head, eye and arm coordination in table tennis. *J. of Sports Sciences vol. 20*, no. 3 (2002), pp. 187–200.
19. Tamaki, T. and Sugino, T. and Yamamoto, M. Measuring ball spin by image registration. In *Proc. of Korea-Japan Joint Workshop on Frontiers of Computer Vision* (2004), pp. 269–274.
20. Wendel, A. and Sabine S. and Martin G. Measuring ball spin in monocular video. In *Proc. of Computer Vision Winter Workshop* (2011), pp. 83–89.
21. Yifeng Z. and Rong X. and Yongsheng Z. and Jianguo W. Real-time spin estimation of ping-pong ball using its natural brand. *IEEE Trans. on Instrumentation and Measurement vol. 64*, no. 8 (2015), pp. 2280–2290.